PTEP

Prog. Theor. Exp. Phys. **2015**, 013D04 (9 pages)
DOI: 10.1093/ptep/ptu180

Changes in rotational characters of one- and two-phonon gamma-vibrational bands in ^{105}Mo

Masayuki Matsuzaki*

Department of Physics, Fukuoka University of Education, Munakata, Fukuoka 811-4192, Japan
*E-mail: matsuza@fukuoka-edu.ac.jp

Received November 21, 2014; Accepted December 17, 2014; Published January 28, 2015

The γ vibration is the most typical low-lying collective motion prevailing in the nuclear chart. But only few one-phonon rotational bands in odd-A nuclei are known. Furthermore, two-phonon states, even the band head, have been observed in a very limited number of nuclides, not only odd-A but also even–even. Among them, that in ^{105}Mo is unique in that Coriolis effects are expected to be stronger than in ^{103}Nb and ^{105}Nb, on which theoretical studies have been reported. The purpose of the present work, then, is to study ^{105}Mo, paying attention to the rotational character change of the one-phonon and two-phonon bands. The particle–vibration coupling model based on the cranking model and the random-phase approximation is used to calculate the vibrational states in rotating odd-A nuclei. The present model reproduces the observed yrast zero-phonon and one-phonon bands well. Emerging general features of the rotational character change from low spin to high spin are elucidated. In particular, the reason why the one-phonon band does not exhibit signature splitting is clarified. The calculated collectivity of the two-phonon states, however, is located higher than observed.

Subject Index D11, D13

1. Introduction

Based on the long history of the physics of the atomic nucleus as a finite quantum many-body system bound by strong interactions, interactions between two, or among three or more, nucleons can nowadays be related to quantum chromodynamics. The interaction thus obtained can be used as an input to large-scale shell-model calculations. On the other hand, from the mean-field picture, density-functional theories that describe ground states of a wide range of nuclides in the nuclear chart are developing. For a class of excited states, the generator-coordinate method is used. Applications of such a framework to light odd-A nuclei have just begun [1].

Aside from this progress, traditional effective models are still indispensable for describing detailed properties of collective excitations. In finite many-body systems, individual particle motions and collective motions are of similar energy scales and, hence, couple to each other. In addition, they are sensitive to the numbers of constituents or the shell filling. Collective vibrations are not necessarily harmonic oscillations and whether multiple excitations exist or not is not trivial.

One of the typical collective motions in medium-heavy nuclei is the γ vibration. However, its double excitation has been identified in a limited number of nuclides such as ^{168}Er [2], ^{166}Er [3, 4], ^{164}Dy [5], ^{232}Th [6], ^{106}Mo [7], ^{104}Mo [8], and ^{138}Nd [9] in even–even nuclei. Among them, ^{168}Er, the one first observed, was studied in terms of various theoretical approaches, as reviewed in Ref. [10].

In odd-A nuclei, the first observation of the two-phonon γ vibration was made in ^{105}Mo [11], on which no theoretical studies have been reported, to the author's knowledge, and to which the present study is devoted. Then, similar excitations were observed in ^{103}Nb [12] and ^{107}Tc [13]. The first realistic calculation on ^{103}Nb [14] was performed in terms of the triaxial projected shell model. After that, the present author made a calculation on this nuclide in terms of the particle–vibration coupling model in Ref. [10].

Quite recently, two-phonon states very similar to those in ^{103}Nb were observed in ^{105}Nb [15]. In these isotopes, candidates of three-phonon states that fed two-phonon bands strongly were also indicated. If their property is confirmed, they are the first three-phonon excitation in deformed nuclei, and may indicate that there is a mechanism that makes odd-A nuclei more favorable for realizing three-phonon γ vibrations than even–even nuclei, although the spectra of odd-A nuclei are thought to be more complex than those of even–even nuclei in general. In Ref. [16], the present author studied these three-phonon candidates while invoking a method to calculate interband $B(E2)$ based on the generalized intensity relation [17]. The result is promising but still not definitive.

Returning to two-phonon states, the odd particle that couples to them in ^{103}Nb and ^{105}Nb is in the $\pi[422]\,5/2^+$ orbital originating from the $g_{9/2}$ subshell, on which Coriolis effects are not very strong. Then, states at finite rotation can still be approximately classified in terms of K, the projection of the angular momentum to the z axis. In contrast, the odd particle in ^{105}Mo is in the $\nu[532]\,5/2^-$ orbital originating from the $h_{11/2}$ subshell, on which Coriolis effects are stronger. Accordingly, the characters of rotational band members would be different. This point is the main concern of the present work.

Throughout this paper the $\hbar = 1$ unit is used.

2. The model and parameters

The particle–vibration coupling (PVC) model based on the cranking model and the random-phase approximation (RPA) is used for calculating eigenstates of odd-A nuclei. In the first step, the one-dimensionally cranked Nilsson plus BCS one-body Hamiltonian is diagonalized,

$$\begin{aligned} h' &= h - \omega_{\rm rot} J_x \\ &= \sum_{\mu} e'_{\mu} a^{\dagger}_{\mu} a_{\mu} + \sum_{\bar{\mu}} e'_{\bar{\mu}} a^{\dagger}_{\bar{\mu}} a_{\bar{\mu}} + \text{const}, \end{aligned} \tag{1}$$

where h is the standard Nilsson plus BCS Hamiltonian. This gives a set of quasiparticle (qp) states. Secondly, we apply the RPA to the residual two-body pairing plus doubly stretched quadrupole–quadrupole interaction between quasiparticles,

$$\begin{aligned} H_{\rm int} &= -\sum_{\tau=1,2} G_{\tau} \tilde{P}^{\dagger}_{\tau} \tilde{P}_{\tau} - \frac{1}{2} \sum_{K=0,1,2} \kappa^{(+)}_{K} Q''^{(+)\dagger}_{K} Q''^{(+)}_{K} - \frac{1}{2} \sum_{K=1,2} \kappa^{(-)}_{K} Q''^{(-)\dagger}_{K} Q''^{(-)}_{K} \\ &= \sum_{n} \omega_n X^{\dagger}_n X_n. \end{aligned} \tag{2}$$

This gives many RPA modes. Cranking and RPA calculations are done in the five major shells, $N_{\rm osc} =$ 2–6 for the neutron and 1–5 for the proton. Among the RPA modes, we choose the γ-vibrational phonons, $n = \gamma$ and $\bar{\gamma}$, with signature $r = \exp(-i\pi\alpha) = 1$ and -1, respectively, which have

outstandingly large $K = 2$ transition amplitudes. Regarding them as elementary excitations, we diagonalize the PVC Hamiltonian:

$$H_{\rm couple}(\gamma) = \sum_{\mu\nu}\Lambda_\gamma(\mu\nu)\left(X^\dagger_\gamma a^\dagger_\mu a_\nu + X_\gamma a^\dagger_\nu a_\mu\right) + \sum_{\mu\bar\nu}\Lambda_{\bar\gamma}(\mu\bar\nu)\left(X^\dagger_{\bar\gamma} a^\dagger_\mu a_{\bar\nu} + X_{\bar\gamma} a^\dagger_{\bar\nu} a_\mu\right) + \text{sig. conj.} \tag{3}$$

These calculations are performed in terms of signature-classified bases, and all the resulting quantities are given as continuous functions of the rotational frequency $\omega_{\rm rot}$. Detailed expressions of these formulations are given in Ref. [10].

Diagonalizations of the PVC Hamiltonian are performed in the model space spanned by 0–4γ basis states, as in Ref. [16]. Here $n\gamma$ basis states designate 1qp $\otimes$ (γ or $\bar\gamma$)^n states. Because there are two types of γ-vibrational phonons, γ and $\bar\gamma$, $(1{\rm qp})_{r=\pm i}\otimes\gamma$ and $(1{\rm qp})_{r=\mp i}\otimes\bar\gamma$ are possible for the 1γ states in the $r = \pm i$ sector. Similarly, there are 3–5 types of 2–4γ basis states, respectively, for each signature. The concrete form of eigenstates with $r = -i$ is given by Eq. (7) in Ref. [16]. That with $r = +i$, obtained by interchanging μ and $\bar\mu$, is given here:

$$\begin{aligned}
|\bar\chi_i\rangle = {} & \sum_{\bar\mu}\psi^{(1)}_i(\bar\mu)\, a^\dagger_{\bar\mu}|\phi\rangle + \sum_{\bar\mu}\psi^{(3)}_i(\bar\mu\gamma)\, a^\dagger_{\bar\mu}X^\dagger_\gamma|\phi\rangle + \sum_{\mu}\psi^{(3)}_i(\mu\bar\gamma)\, a^\dagger_{\mu}X^\dagger_{\bar\gamma}|\phi\rangle \\
& + \sum_{\bar\mu}\psi^{(5)}_i(\bar\mu\gamma\gamma)\frac{1}{\sqrt{2}}\, a^\dagger_{\bar\mu}\left(X^\dagger_\gamma\right)^2|\phi\rangle + \sum_{\bar\mu}\psi^{(5)}_i(\bar\mu\bar\gamma\bar\gamma)\frac{1}{\sqrt{2}}\, a^\dagger_{\bar\mu}\left(X^\dagger_{\bar\gamma}\right)^2|\phi\rangle \\
& + \sum_{\mu}\psi^{(5)}_i(\mu\gamma\bar\gamma)\, a^\dagger_{\mu}X^\dagger_\gamma X^\dagger_{\bar\gamma}|\phi\rangle \\
& + \sum_{\bar\mu}\psi^{(7)}_i(\bar\mu\gamma\gamma\gamma)\frac{1}{\sqrt{3!}}\, a^\dagger_{\bar\mu}\left(X^\dagger_\gamma\right)^3|\phi\rangle + \sum_{\mu}\psi^{(7)}_i(\mu\bar\gamma\bar\gamma\bar\gamma)\frac{1}{\sqrt{3!}}\, a^\dagger_{\mu}\left(X^\dagger_{\bar\gamma}\right)^3|\phi\rangle \\
& + \sum_{\mu}\psi^{(7)}_i(\mu\gamma\gamma\bar\gamma)\frac{1}{\sqrt{2}}\, a^\dagger_{\mu}\left(X^\dagger_\gamma\right)^2X^\dagger_{\bar\gamma}|\phi\rangle + \sum_{\bar\mu}\psi^{(7)}_i(\bar\mu\gamma\bar\gamma\bar\gamma)\frac{1}{\sqrt{2}}\, a^\dagger_{\bar\mu}X^\dagger_{\bar\gamma}\left(X^\dagger_{\bar\gamma}\right)^2|\phi\rangle \\
& + \sum_{\bar\mu}\psi^{(9)}_i(\bar\mu\gamma\gamma\gamma\gamma)\frac{1}{\sqrt{4!}}\, a^\dagger_{\bar\mu}\left(X^\dagger_\gamma\right)^4|\phi\rangle + \sum_{\bar\mu}\psi^{(9)}_i(\bar\mu\bar\gamma\bar\gamma\bar\gamma\bar\gamma)\frac{1}{\sqrt{4!}}\, a^\dagger_{\bar\mu}\left(X^\dagger_{\bar\gamma}\right)^4|\phi\rangle \\
& + \sum_{\mu}\psi^{(9)}_i(\mu\gamma\gamma\gamma\bar\gamma)\frac{1}{\sqrt{3!}}\, a^\dagger_{\mu}\left(X^\dagger_\gamma\right)^3X^\dagger_{\bar\gamma}|\phi\rangle + \sum_{\mu}\psi^{(9)}_i(\mu\gamma\bar\gamma\bar\gamma\bar\gamma)\frac{1}{\sqrt{3!}}\, a^\dagger_{\mu}X^\dagger_\gamma\left(X^\dagger_{\bar\gamma}\right)^3|\phi\rangle \\
& + \sum_{\bar\mu}\psi^{(9)}_i(\bar\mu\gamma\gamma\bar\gamma\bar\gamma)\frac{1}{2}\, a^\dagger_{\bar\mu}\left(X^\dagger_\gamma\right)^2\left(X^\dagger_{\bar\gamma}\right)^2|\phi\rangle .
\end{aligned} \tag{4}$$

In the present work, μ and $\bar\mu$ run 21 states in the neutron $N_{\rm osc} = 5$ shell.

The bands in ^{105}Mo studied in the present work are the yrast $\nu[532]\,5/2^-$ band and corresponding single- and double-γ-vibrational bands. In the following, qp states at finite γ and $\omega_{\rm rot}$ are also designated by the dominant asymptotic states. The lowest qp states with the dominant $\nu[532]\,5/2^-$ component are denoted by $\bar\mu = \bar 1$ and $\mu = 1$ for $r = +i$ and $r = -i$, respectively. These are the dominant components of the lowest (zero-phonon) PVC eigenstate in each signature. Then the two dominant components of the one-phonon PVC eigenstates are $\bar 1\otimes\gamma$ and $1\otimes\bar\gamma$ for $r = +i$, and $1\otimes\gamma$ and $\bar 1\otimes\bar\gamma$ for $r = -i$. Straightforwardly, those of the two-phonon in $r = +i$ are $\bar 1\otimes\gamma\gamma$, $\bar 1\otimes\bar\gamma\bar\gamma$, and $1\otimes\gamma\bar\gamma$, while those in $r = -i$ are $1\otimes\gamma\gamma$, $1\otimes\bar\gamma\bar\gamma$, and $\bar 1\otimes\gamma\bar\gamma$. The sum of the fractions of these main components defines the collectivity of calculated eigenstates.

The parameters entered into the calculation are chosen in a manner similar to the case of Refs. [10] and [16]. Concretely, the pairing gaps, $\Delta_n = 1.05$ MeV and $\Delta_p = 0.85$ MeV, are those widely used for both even- and odd-A nuclides in this mass region [7,12]. The quadrupole deformation, $\epsilon_2 = 0.3254$, is the same as that adopted for the isobar ^{105}Nb in Ref. [16]. The triaxial deformation γ is chosen so that the calculated signature splitting $\Delta e'$ between the lowest PVC eigenstates reproduces the overall features of the observed one. The resulting value, $\gamma = -10^\circ$, is again the same as that for ^{105}Nb. For the quadrupole interaction strengths, the ones examined in the first attempt were those that reproduce the observed γ-vibrational energy ω_γ, 0.8121 MeV of ^{104}Mo [8], 0.7104 MeV of ^{106}Mo [7], or their average, in the RPA calculation for the even–even core state at each γ, as in previous calculations [10,16,18–20]. But these were unsuccessful because the $\nu[541]\,3/2^-$ qp-dominant state is slightly higher than the one-phonon states in the PVC calculation and the former pushes down the latter. This contradicts the observed situation that the γ-vibrational energy of ^{105}Mo is higher than those of ^{104}Mo and ^{106}Mo; see Fig. 10 of Ref. [11]. To reproduce this phenomenologically, we adopt the interaction strengths that give $\omega_\gamma = 1.0$ MeV in the RPA calculation for the even–even core and consequently bring the one-phonon states higher than the $\nu[541]\,3/2^-$-dominant state in the PVC calculation at $\omega_{\rm rot} = 0$. After rotation sets in, the calculated ω_γ and $\omega_{\bar\gamma}$ in the RPA calculation almost degenerate up to $\omega_{\rm rot} = 0.3$ MeV, then, at this rotational frequency, the γ with $r = +1$ is crossed by the steeply down-sloping $(\nu[532]\,5/2^-)^2$ state. This crossing produces irregularities in the PVC calculation. The configuration with this alignment is the s-band state in this mass region; it would become the yrast in the even–even core when its Routhian reaches 0 at higher $\omega_{\rm rot}$, although this crossing is blocked in the odd-A system, with one of the $\nu[532]\,5/2^-$ signature-partner pair being already occupied. Therefore, irregularities at $\omega_{\rm rot} = 0.3$ MeV are artifacts of the model and should be ignored. After this crossing, ω_γ is slightly larger than $\omega_{\bar\gamma}$.

3. Results and discussion

The Routhians in the one-phonon region are shown in Figs. 1(a) for $r = +i$ and (b) for $r = -i$. There are three eigenstates around $e' = 1.8$ MeV at $\omega_{\rm rot} \sim 0$ in both signature sectors. If the static triaxial deformation that mixes the K quantum number is ignored, the second, third, and fourth states are the $\nu[541]\,3/2^-$, the $K = \Omega - 2 = 1/2\,\gamma$ vibration, and the $K = \Omega + 2 = 9/2\,\gamma$ vibration, respectively. Hereafter, j and Ω are the single-particle angular momentum and its projection to the z axis.

In the single-j approximation effective for high-j cases, the favored state ($r = +i$ in the present case) is written as $|{\rm f}_\Omega\rangle = \frac{1}{\sqrt{2}}\,(|\Omega\rangle + |-\Omega\rangle)$ while the unfavored state ($r = -i$ in the present case) is $|{\rm u}_\Omega\rangle = \frac{1}{\sqrt{2}}\,(|\Omega\rangle - |-\Omega\rangle)$ at $\omega_{\rm rot} = 0$, aside from overall phases. Therefore, those with $\Omega = 1/2$ have diagonal matrix elements of J_x and consequently their Routhians, eigenvalues of $h' = h - \omega_{\rm rot} J_x$, split as soon as rotation sets in. This splitting propagates to other states through the Ω mixing at finite $\omega_{\rm rot}$. This is the basic mechanism of the signature splitting. In addition, when triaxial deformation, represented by the term proportional to $Q_2^{(+)} = \frac{1}{\sqrt{2}}\,(Q_{22} + Q_{2-2})$ in h, and/or couplings to the γ vibration exist, $\Omega = 3/2$ states also split through, e.g., $\langle 3/2|Q_{22}|-1/2\rangle \times \langle -1/2|J_x|1/2\rangle \times \langle 1/2|Q_{22}|-3/2\rangle$. This is the reason why both the noncollective second and collective third states exhibit finite alignments $= -de'/d\omega_{\rm rot}$ at $\omega_{\rm rot} = 0$ and interact with each other at finite $\omega_{\rm rot}$. Because the mutual repulsion extends over a wide range of $\omega_{\rm rot}$, the third (originally lower one-phonon) state is pushed up and also interacts with the fourth (originally upper one-phonon)

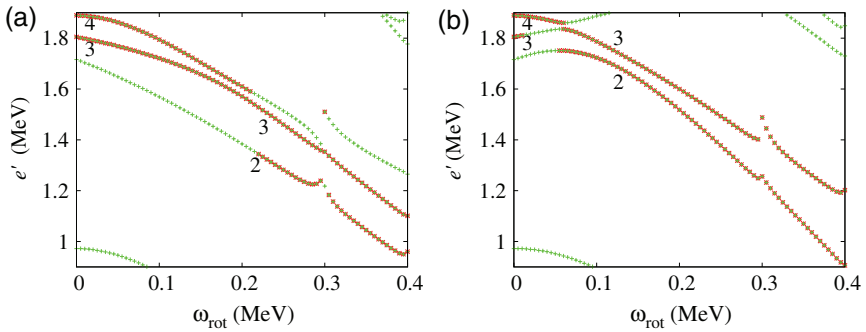

Fig. 1. Routhians of all calculated PVC states in the region of one-phonon bands are shown by green +, (a) in the $r = +i$ sector and (b) in the $r = -i$ sector. Those with more than 50% collective fraction are emphasized by red $\times$. The labels attached designate the numbers, i in Eq. (4) in the present article for $r = +i$ and in Eq. (7) in Ref. [16] for $-i$, enumerated from the lowest. Note that the lowest state seen only at small $\omega_{\rm rot}$ in each figure is the yrast zero-phonon state.

state. Then, at $\omega_{\rm rot} > 0.2$ MeV, the third state carries the character of the upper one-phonon state in $r = +i$, whereas the effect of the noncollective state is only local in $r = -i$.

Aside from this perturbation from the noncollective state, the collective states show the pattern, common to the previous cases of ^{103}Nb and ^{105}Nb, that the lower one-phonon state has $K = \Omega - 2$ with a finite alignment (positive for the favored and negative for the unfavored) and the upper one has $K = \Omega + 2$ with negligible alignment for small $\omega_{\rm rot}$; see Fig. 3(a) in Ref. [16]. For example, in the $r = -i$ sector, both of them are dominantly composed of the $1 \otimes \gamma$ and $\bar{1} \otimes \bar{\gamma}$ basis states. Two orthogonal combinations of them with similar magnitudes form the eigenstates with $K = \Omega - 2$ and $\Omega + 2$, as discussed in Ref. [16]. This pattern is preserved in the whole calculated range of $\omega_{\rm rot}$ in the cases of ^{103}Nb and ^{105}Nb with the $\pi g_{9/2}$ odd particle with small signature splittings studied there.

In the present case of ^{105}Mo with the higher-j, $\nu h_{11/2}$, odd particle, in contrast, stronger Coriolis interactions change their characters as $\omega_{\rm rot}$ increases. Actually, the slopes of their Routhians are twice those of ^{103}Nb and ^{105}Nb. Because the signature splitting between the 1 and $\bar{1}$ basis states is significantly larger than that between γ and $\bar{\gamma}$, the $\bar{1} \otimes \bar{\gamma}$ component becomes dominant in the lower one-phonon state while the $1 \otimes \gamma$ component becomes dominant in the upper one in the $r = -i$ sector, for instance.

This character change caused by the Coriolis K mixing can be clearly seen in the wave function shown in Fig. 2 for $r = -i$. Aside from the abrupt change brought about by the crossing with the noncollective state at around $\omega_{\rm rot} = 0.06$ MeV, the $1 \otimes \gamma$ component becomes dominant in the upper one-phonon state at high $\omega_{\rm rot}$. The schematic behavior of the collective states is depicted in Fig. 3. This figure clearly explains the reason why the observed one-phonon band does not exhibit signature splitting in contrast with the yrast zero-phonon band: The observed one-phonon band with the $K = \Omega + 2$ band head does not show signature splitting at $\omega_{\rm rot} \sim 0$ because of the high K, as argued in Ref. [16]. Additionally, at finite $\omega_{\rm rot}$, the $r = +i$ and $r = -i$ sequences of the band consist dominantly of $1 \otimes \bar{\gamma}$ and $1 \otimes \gamma$, respectively; hence, the splitting between them is essentially the difference $\omega_\gamma - \omega_{\bar{\gamma}}$, which is much smaller than the splitting in the yrast zero-phonon band. When $r = -i$ is favored, as in the $g_{9/2}$ and $i_{13/2}$ cases, 1 and $\bar{1}$ in the figure should be interchanged.

The calculated zero- and one-phonon states are compared quantitatively with the observed ones. The reference rotating frame to which the data are converted is determined in two steps. First, the Harris parameters are determined to fit the ground band up to 10^+ of ^{106}Mo as $\mathcal{J}_0 = 18.08\,\text{MeV}^{-1}$

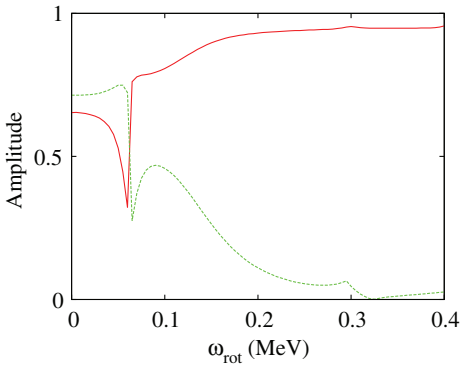

Fig. 2. Amplitudes of the dominant components $|\psi_i^{(3)}(1\gamma)|$ (red solid) and $|\psi_i^{(3)}(\bar{1}\bar{\gamma})|$ (green dashed) in the upper ($i = 3$ at $\omega_{\rm rot} > 0.06\,{\rm MeV}$) one-phonon band in the $r = -i$ sector.

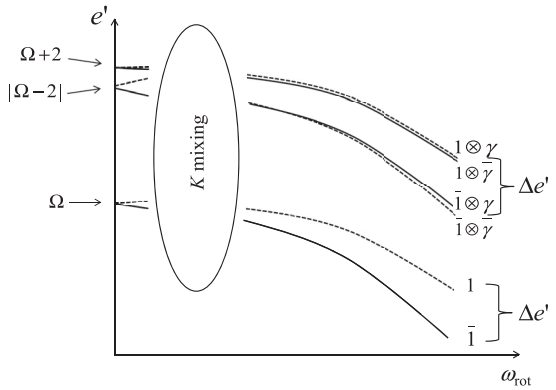

Fig. 3. Schematic drawing of the character change of the zero- and one-phonon bands from the K scheme to the signature scheme caused by the Coriolis K mixing.

and $\mathcal{J}_1 = 43.21\,{\rm MeV}^{-3}$. In the second step, the origin of this frame must be shifted in order to be compared with states in the odd-A system. Usually this overall shift is given by the pairing gap, in the present case $\Delta_n = 1.05\,{\rm MeV}$, in the cranking calculation. In the present calculation, however, the cranking model is extended to the PVC model and this produces a downward shift of the Routhian of the lowest state, 0.078 MeV at $\omega_{\rm rot} = 0$. Accordingly, the overall shift is determined to be 0.972 MeV. The result is shown in Fig. 4. This shows that the zero- and one-phonon states are reproduced well.

Now we proceed to the two-phonon states. How their calculated collectivity distributes is shown in Fig. 5 for $r = -i$ together with the zero- and one-phonon states at four $\omega_{\rm rot}$ values. These figures show that the locations of the one-phonon and two-phonon states are harmonic; at least, their centers of the collective strength are seen. Experimentally, however, an anharmonicity, $E_{2\gamma}/E_{1\gamma} = 1.76$, has been reported, in contrast to the harmonic spectra in the adjacent even–even isotopes, ^{104}Mo [8] and ^{106}Mo [7]. Note here that an anharmonic $E_{2\gamma}$ in ^{106}Mo was cited in Ref. [11], referring to Ref. [21], but it is a misciting of the band-head energy of another band. Reference [21] reported the same harmonic value. These data suggest an unknown mechanism to produce anharmonicity proper to odd-A systems, different from that discussed for even–even nuclei from a microscopic theoretical point of view in Refs. [23–25].

More closely, their Routhians are shown in Figs. 6(a) for $r = +i$ and (b) for $r = -i$ as continuous functions of $\omega_{\rm rot}$. As in the cases of ^{103}Nb and ^{105}Nb, three sequences keep collectivity in the whole calculated range of $\omega_{\rm rot}$, although they are located in the region with larger level density. The lower

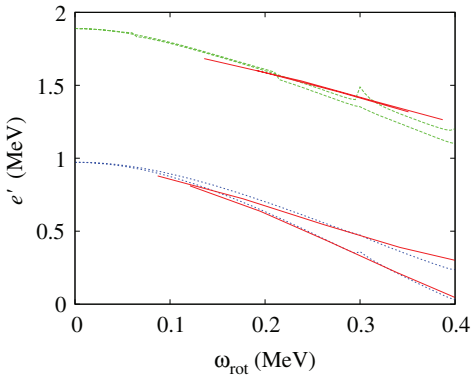

Fig. 4. Routhians of calculated zero-phonon (blue dotted) and upper ($K = \Omega + 2$) one-phonon (green dashed) bands are compared with the corresponding data (red solid) converted to the rotating frame by using the Harris parameters $\mathcal{J}_0 = 18.08\,\mathrm{MeV}^{-1}$ and $\mathcal{J}_1 = 43.21\,\mathrm{MeV}^{-3}$, which fit the yrast band of ^{106}Mo [8]. Thick and thin curves designate $r = +i$ and $-i$, respectively.

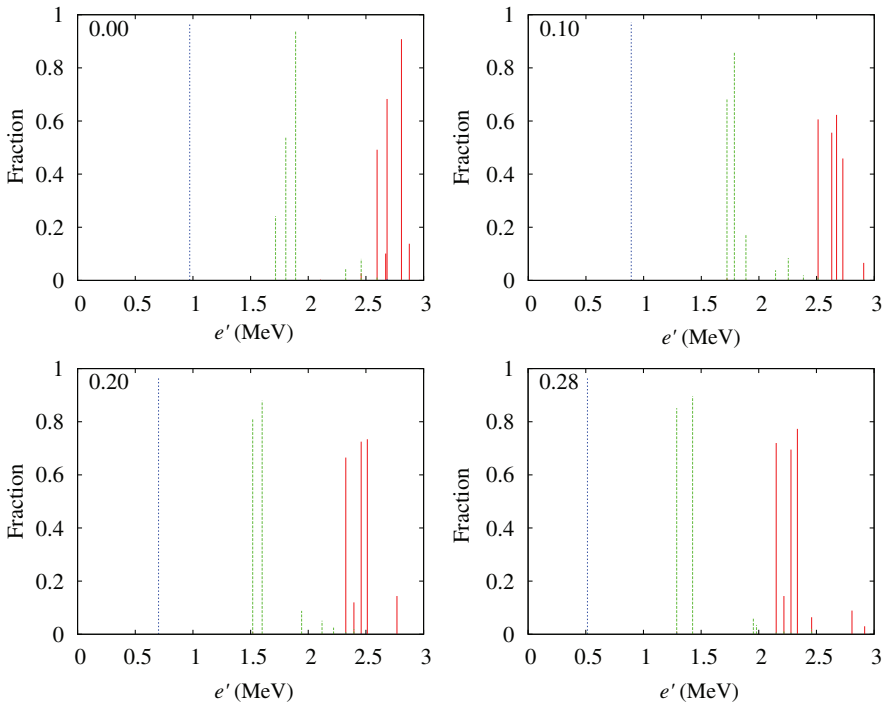

Fig. 5. Distribution of the collective fraction (probability in the wave function) of the zero-, one-, and two-phonon components in the $r = -i$ sector, $|\psi^{(1)}(1)|^2$ (blue dotted), $|\psi^{(3)}(1\gamma)|^2 + |\psi^{(3)}(\bar{1}\bar{\gamma})|^2$ (green dashed), and $|\psi^{(5)}(1\gamma\gamma)|^2 + |\psi^{(5)}(1\bar{\gamma}\bar{\gamma})|^2 + |\psi^{(5)}(\bar{1}\gamma\bar{\gamma})|^2$ (red solid), respectively, at $\omega_{\mathrm{rot}} = 0$, 0.1, 0.2, and 0.28 MeV.

one is of $K = |\Omega - 4| = 3/2$, the medium one is of $K = \Omega = 5/2$, and the upper one is of $K = \Omega + 4 = 13/2$ at $\omega_{\mathrm{rot}} \sim 0$. Experimentally, the band head was assigned as $K = 13/2$ and only two states in each signature were observed. They are represented by a point in the Routhian diagram for each signature, as indicated by red filled squares in Fig. 6.

The locations of the highest peaks of each phonon number in Fig. 5 for $\omega_{\mathrm{rot}} = 0$ do not account for the observed anharmonicity at the band head. The calculated Routhians of the zero-phonon, (upper) one-phonon, and (upper) two-phonon states at $\omega_{\mathrm{rot}} = 0$ are (1.050, 2.050, 3.050) MeV without PVC

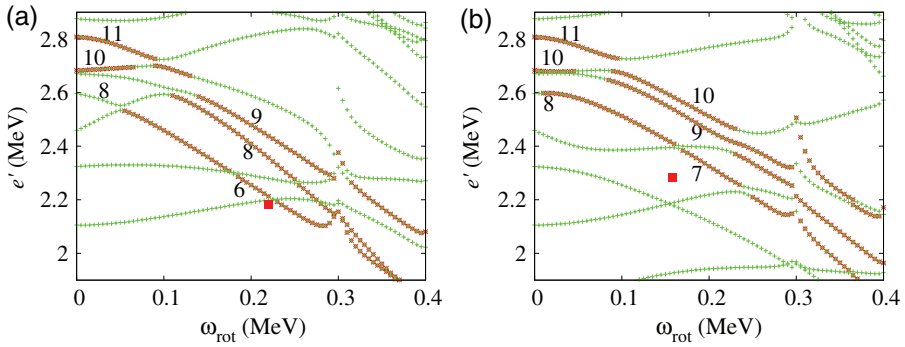

Fig. 6. The same as Fig. 1 but in the region of two-phonon bands. The corresponding data (red filled square) converted to the rotating frame are also shown.

(not shown), and (0.972, 1.890, 2.808) MeV with PVC, respectively. However, at finite $\omega_{\rm rot}$ where actual transitions are observed, the Coriolis effect is significant in the present high-j case and calculated states look like in the signature scheme with mixed K. Inspection of the wave functions indicates that the dominant components are $\bar{1} \otimes \gamma\gamma$ for the lower, $\bar{1} \otimes \bar{\gamma}\bar{\gamma}$ for the medium, and $1 \otimes \gamma\bar{\gamma}$ for the upper in the $r = +i$ sector, while they are $\bar{1} \otimes \gamma\bar{\gamma}$ for the lower, $1 \otimes \bar{\gamma}\bar{\gamma}$ for the medium, and $1 \otimes \gamma\gamma$ for the upper in the $r = -i$ sector. Again, this proves that the order of the collective states is ruled by the signature splitting between the 1 and $\bar{1}$ basis states, as in the one-phonon states in Fig. 3. This indicates that their connection to the band head with fairly pure K is not trivial.

Thus, a natural criterion to choose the state to be identified with (the main component of) the observed one is the largest collectivity, as argued in the three-phonon-candidate cases in Ref. [16], because it is generally expected that the most collective sequence connected by strong $E2$ transitions would be observed. Actually, the upper one, identified with the observed one at the band head, is the most collective at $\omega_{\rm rot} = 0$ because its high-K property prevents it from mixing with other states. However, three sequences begin sharing similar collectivities as soon as rotation sets in. As in the three-phonon case, the state with the highest K effectively has the highest j and, accordingly, feels the strongest Coriolis force as $\omega_{\rm rot}$ increases. Then, it is expected that band members that have large overlaps with the most collective eleventh state with the highest K at $\omega_{\rm rot} \sim 0$ would be energetically lowered by reducing K as $\omega_{\rm rot}$ increases and appear at lower Routhians through band crossing(s). The observed transitions are located near ($r = +i$) or even lower than ($r = -i$) the lowest calculated two-phonon states. However, lowering of the location of collectivity to these lowest states in the present calculation is insufficient, in contrast to the three-phonon case, although j is larger. Therefore, it is difficult to establish the mapping between them.

4. Conclusions

To conclude, the yrast (zero-phonon) $\nu[532]\,5/2^-$ and the one- and two-phonon γ-vibrational bands in ^{105}Mo have been calculated in the particle–vibration coupling model based on the cranking model and the random-phase approximation, paying attention to the rotational effects on the spectra, in comparison to the lower-j cases of ^{103}Nb and ^{105}Nb studied in previous work.

The zero- and one-phonon bands have been reproduced well. In particular, the rotational character change from the K scheme to the signature scheme through the Coriolis K mixing in the one-phonon states is stressed. This naturally accounts for the reason why the observed one-phonon band does not exhibit signature splitting, in contrast to the yrast zero-phonon band. A specific feature of the data is

that the two-phonon states show anharmonicity in the spectra that is absent in ^{103}Nb, ^{105}Nb, ^{104}Mo, and ^{106}Mo. This fact suggests that there exists an unknown mechanism to produce anharmonicity proper to high-j odd-A nuclei. The particle–vibration coupling pushes them down, but the result is still harmonic with a slightly reduced interval at $\omega_{\rm rot} = 0$. A possibility applicable to finite $\omega_{\rm rot}$, inspired from the previous calculation for the three-phonon-candidate states in ^{103}Nb and ^{105}Nb, is that the continuation of the highest-lying two-phonon state with the highest K would be energetically lowered by a strong Coriolis force. In the present calculation, however, its lowering is insufficient.

References

[1] B. Bally, B. Avez, M. Bender, and P.-H. Heenen, Phys. Rev. Lett. **113**, 162501 (2014).
[2] W. F. Davidson et al., J. Phys. G **7**, 455 (1981); **7**, 843 (1981) [addendum].
[3] C. Fahlander et al., Phys. Lett. B **388**, 475 (1996).
[4] P. E. Garrett et al., Phys. Rev. Lett. **78**, 4545 (1997).
[5] F. Corminboeuf et al., Phys. Rev. C **56**, R1201 (1997).
[6] W. Korten et al., Phys. Lett. B **317**, 19 (1993).
[7] A. Guessous et al., Phys. Rev. Lett. **75**, 2280 (1995).
[8] A. Guessous et al., Phys. Rev. C **53**, 1191 (1996).
[9] H. J. Li et al., Phys. Rev. C **87**, 057303 (2013).
[10] M. Matsuzaki, Phys. Rev. C **83**, 054320 (2011).
[11] H. B. Ding et al., Phys. Rev. C **74**, 054301 (2006).
[12] J.-G. Wang et al., Phys. Lett. B **675**, 420 (2009).
[13] L. Gu et al., Chin. Phys. Lett. **26**, 092502 (2009).
[14] J. A. Sheikh, G. H. Bhat, Y. Sun, and R. Palit, Phys. Lett. B **688**, 305 (2010).
[15] H. J. Li et al., Phys. Rev. C **88**, 054311 (2013).
[16] M. Matsuzaki, Phys. Rev. C **90**, 044313 (2014).
[17] Y. R. Shimizu and T. Nakatsukasa, Nucl. Phys. A **611**, 22 (1996).
[18] M. Matsuzaki, Y. R. Shimizu, and K. Matsuyanagi, Prog. Theor. Phys. **77**, 1302 (1987).
[19] M. Matsuzaki, Y. R. Shimizu, and K. Matsuyanagi, Prog. Theor. Phys. **79**, 836 (1988).
[20] G. Gervais et al., Nucl. Phys. A **624**, 257 (1997).
[21] R. Q. Xu et al., Chin. Phys. Lett. **19**, 180 (2002).
[22] H. Hua et al., Phys. Rev. C **69**, 014317 (2004).
[23] M. Matsuo and K. Matsuyanagi, Prog. Theor. Phys. **74**, 1227 (1985).
[24] M. Matsuo and K. Matsuyanagi, Prog. Theor. Phys. **76**, 93 (1986).
[25] M. Matsuo and K. Matsuyanagi, Prog. Theor. Phys. **78**, 591 (1987).